Anti-Correlated Spectral Motion in Bisphthalocyanines: Evidence for Vibrational Modulation of Electronic Mixing

Bradley S. Prall,[†] Dilworth Y. Parkinson,[†] Naoto Ishikawa,[‡] and Graham R. Fleming*[,†]

Department of Chemistry, University of California, Berkeley, and Physical Biosciences Division, Lawrence Berkeley National Laboratory, Berkeley, California 94720, and Department of Applied Chemistry, Chuo University, 1-13-27 Kasuga, Bunkyo-ku, Tokyo 112-8551, Japan

Received: July 29, 2005; In Final Form: September 29, 2005

We exploit a coherently excited nuclear wave packet to study nuclear motion modulation of electronic structure in a metal bridged phthalocyanine dimer, lutetium bisphthalocyanine, which displays two visible absorption bands. We find that the nuclear coordinate influences the energies of the underlying exciton and charge resonance states as well as their interaction; the interplay of the various couplings creates unusual anti-correlated spectral motion in the two bands. Excited state relaxation dynamics are the same regardless of which transition is pumped, with decay time constants of 1.5 and 11 ps. The dynamics are analyzed using a three-state kinetic model after relaxation from one or two additional states faster than the experimental time resolution of 50−100 fs.

Introduction

The modification of chromophore optical and electronic properties such as redox potential through interactions with other chromophores has been exploited throughout natural photosynthetic systems. Perhaps the best studied, but still incompletely understood, system is the special pair of the purple bacterial reaction center.[1,2] For example, it has recently been proposed that the remarkable blue shift of the lowest excited state with increase of temperature in the bacterial reaction center arises from coupling of the excitonic state and a dark charge transfer state.[3] Clearly, such interactions can be strongly influenced by nuclear motions within the dimer, which in turn can lead to strong modulation of the optical and dynamical properties of the system.

Extensive studies of nuclear motion excited by ultrashort light pulses in monomeric systems[4−17] do not provide much guidance for the interplay between electronic structure and nuclear motion in molecular complexes. Nevertheless, it is intuitively clear that the electronic structure could be strongly influenced by motions that, for example, alter the separation of two chromophores. In this paper, we study such effects in a phthalocyanine dimer, $Lu(Pc)_2^-$, where a single lutetium atom acts as a bridge between the two phthalocyanine rings.[18] In this system, the single monomer band is split into two bands,[19] with a gap between them which depends on the intermolecular distance, which in turn depends on the metal. This phthalocyanine dimer provides a well-defined system with which to explore the electronic mixing of monomer states and the role of nuclear motions in modulating the electronic coupling.

By exploiting a coherently excited nuclear wave packet, we observe the nuclear dependence of the electronic mixing between the exciton and charge resonance states which appear in electronic structure calculations.[20,21] This change in mixing is manifested in our pump−probe measurements as unusual anti-correlated wave packet dynamics for the two dipole-allowed states. The anti-correlated dynamics match previous studies which showed a π phase difference in the oscillations in one- versus two-color photon echo peak shift signals (1C3PEPS and 2C3PEPS).[22] Because 2C3PEPS measures electronic interaction between states, that observation supports the idea that nuclear dynamics modify the electronic interaction in this dimer system.[23]

On the basis of our pump−probe data, we develop a simple model through which the change in mixing induced by molecular motion can be estimated. This model is only a first step toward understanding our experimental data, but it is able to qualitatively explain all of the patterns we observe, and it may have relevance for natural dimer systems, such as the special pair of purple photosynthetic bacteria,[24−26] where protein motions may modulate the electronic coupling between the two monomers.

Experimental Section

Experiments were performed with laser pulses from a home-built 1 kHz, 40 fs Ti:sapphire regenerative amplifier seeded by a commercial oscillator (Femtosource Compact Pro, Femtolasers Inc.). About 6 mW of the amplifier output was used to pump a commercial optical parametric amplifier (Coherent 9450), generating tunable pump pulses of approximately 35 fs duration. White light probe pulses were generated with 2 mW of the amplifier output and a sapphire window. Residual 800 nm light was removed from the white light using a 750 nm short-pass filter. A strong negative solvent response feature near time zero was used to correct for the chirp of the white light probe. The trace at each wavelength was shifted in time on the basis of a quadratic function of wavelength aligned with the negative feature. The uncertainty in the time zero at any wavelength is less than the duration of the pump pulse. All experiments were performed at magic angle polarization to eliminate anisotropy effects.[27]

Long time traces (to 50 ps) were wavelength resolved using a 1 nm band-pass monochromator and detected on a photodiode using standard lock-in techniques. Short time traces (to 2.5 ps)

* To whom correspondence should be addressed. E-mail: GRFleming@lbl.gov.
[†] University of California, Berkeley, and Lawrence Berkeley National Laboratory.
[‡] Chuo University.

10.1021/jp054225d CCC: $30.25
Published on Web 11/10/2005

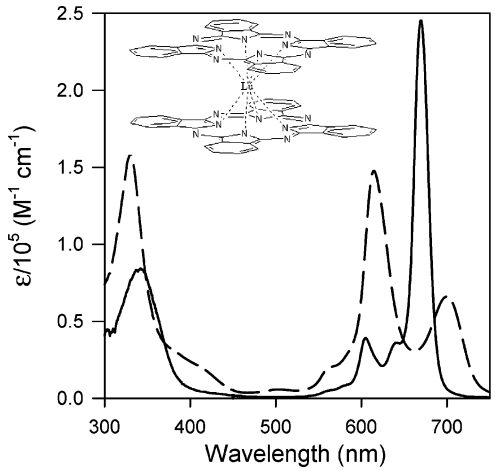

Figure 1. Absorption spectra of the monomer LuPcAc (solid line) and the dimer $LuPc_2^-$ (dashed line). The inset shows the structure of $LuPc_2^-$.

were recorded using an Ocean Optics S2000 fiber optic spectrometer with the high speed driver and 2 MHz PCI card. For this configuration, the chopper phase had to be determined from the data, which limited its use to time regions with strong signal for at least one wavelength. $LuPc_2^-$ was dissolved in basic ethanol and flowed through a room temperature 500 μm quartz cell.

Results

Pump−probe experiments on the short time dynamics of $LuPc_2^-$ were performed with pump wavelengths of 615 and 700 nm, which match the peaks of two bands in the linear absorption spectrum, as seen in Figure 1. The time-resolved spectra for the two pump wavelengths are shown in Figure 2. The data are plotted in terms of the relative change in transmittance, or $\Delta T/T$, which is linearly proportional to the change in absorbance for the small values of $\Delta T/T$ which we observe. Surprisingly, aside from differences in the absolute magnitude of $\Delta T/T$ due to different pump intensities, the time-resolved spectra are essentially identical for the two different pump wavelengths.

The most striking feature of the data presented in Figure 2 is the strong anti-correlated 210 fs oscillations. We use the term anti-correlated to mean that the modulation on the red side of the high energy band is exactly out of phase with the modulation of the red side of the low energy band but is in phase with the modulation of the blue side of the low energy band. A comparison of the oscillations observed for excitation at 615 nm and probed at 630 and 695 nm (i.e., on the red side of the high energy band and on the blue side of the lower energy band, respectively) is shown in Figure 3A. This figure displays the residuals after removing the decay components. These residuals are essentially identical, suggesting that the modulations have the same source.

In addition to the anti-correlated motion, another intriguing aspect of the data is that the overall phase of the oscillation is independent of the initial state populated. This is highlighted in Figure 3B and C, where the signal for probe wavelengths of 630 and 695 nm is compared for pump wavelengths of 615 and 700 nm. As this figure illustrates, regardless of pump wavelength, the overall exponential decays are identical and the modulations are identical in amplitude, frequency, phase, and damping relative to the strength of the signal.

The residuals, after removing the decay components at each wavelength, were fit to a single damped cosine with variable amplitude, phase, period, and damping time. These fits indicate that the oscillations in the two bands are centered at 615 and 715 nm, respectively, with π phase changes around these points. The period of the beats for all wavelengths was 207−211 fs. The damping time varied from ∼1.2 ps near the points of strongest modulation to ∼600 fs farther from the band centers.

The decay of the signal is not uniform across the band, indicating the presence of multiple states in the decay process. Figure 4 presents data from long time traces with the pump set to 615 nm. After the initial decay, a negative $\Delta T/T$ associated with an absorption process clearly appears around 640 nm. The entire spectrum then decays on a time scale of tens of picoseconds.

Fitting the short time decay at each wavelength to a single exponential decay and a static component yields a range of time scales between 1 and 1.6 ps. The time constant is about 1.5 ps in the regions where it comprises a major part of the decay; fixing the decay time to 1.5 ps for all frequencies yields fits of the same quality except in the region around 615 nm, where an additional fast decay (∼100 fs) appears when pumping either the 615 or 700 nm bands. The static component is associated with the ∼11 ps time scale found in the long time traces. The amplitudes of the exponential and static components of the fit as a function of wavelength are shown in Figure 5. The

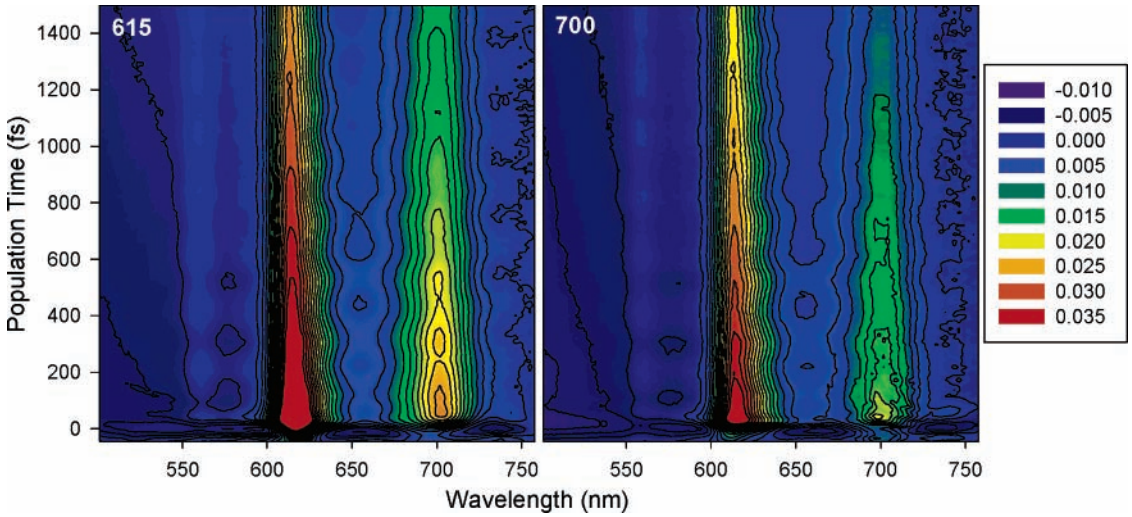

Figure 2. Wavelength-resolved $\Delta T/T$ for $LuPc_2^-$ when pumping (left panel) the $|2E+\rangle$ state at 615 nm and (right panel) the $|1E+\rangle$ state at 700 nm. The strong positive response observed around 615 and 700 nm is characteristic of ground state bleach. Exited state absorption is clearly visible as the negative response from 500 to 600 nm.

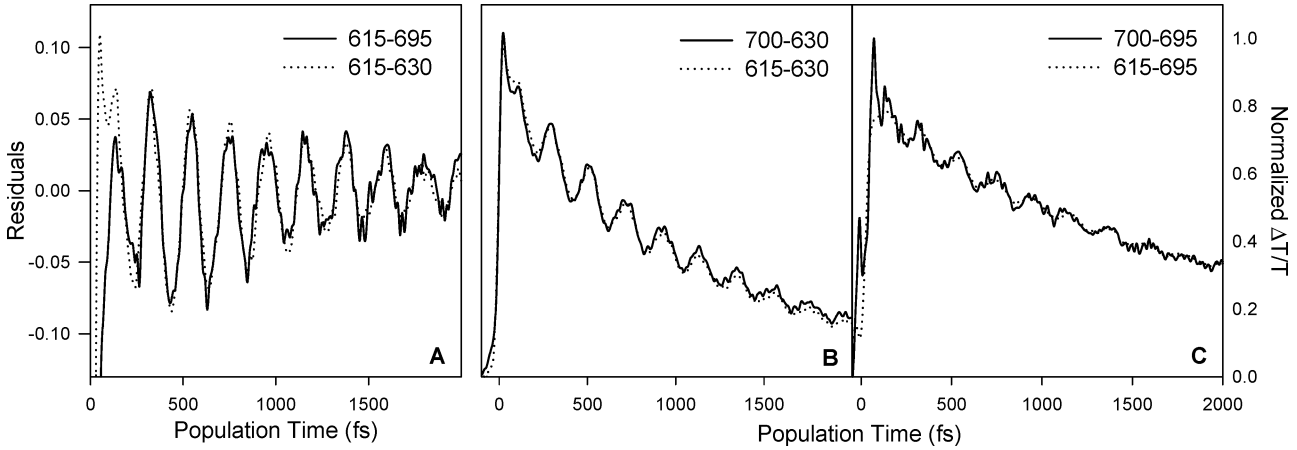

Figure 3. (A) Scaled residuals after fitting experimental traces to an exponential and a static component. These traces correspond to pumping the $|2E+\rangle$ state at 615 nm and probing the $|2E+\rangle$ and $|1E+\rangle$ states at 630 and 695 nm, respectively. These wavelengths correspond to probing the red side of the upper state and the blue side of the lower state. (B and C) Experimental traces for pumping both the $|2E+\rangle$ state at 615 nm and the $|1E+\rangle$ state at 700 nm when probing the $|2E+\rangle$ state at 630 nm, to the red of the band center (panel B), or the $|1E+\rangle$ state at 695 nm, to the blue of the band center (panel C).

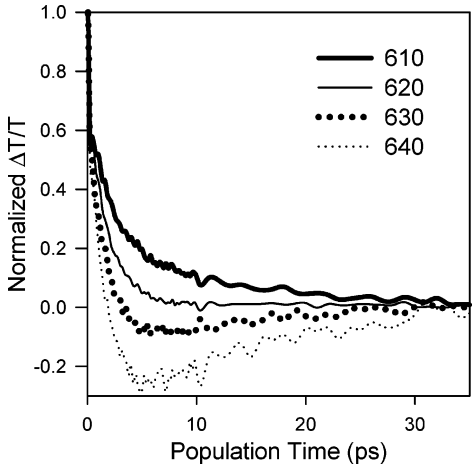

Figure 4. Wavelength-resolved $\Delta T/T$ for pumping the $|2E+\rangle$ state at 615 nm and probing at four wavelengths near the $|2E+\rangle$ state: 610, 620, 630, and 640 nm. The band center is ~615 nm.

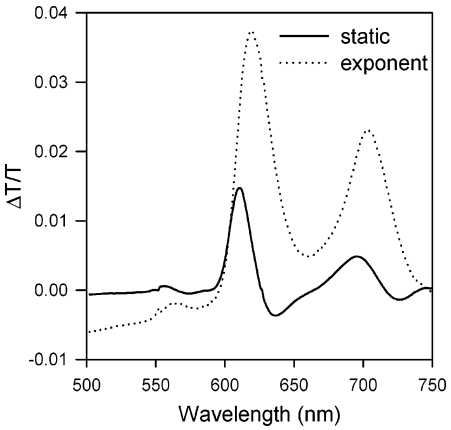

Figure 5. Amplitudes associated with the 1.5 ps exponential and the static offset components which were used to fit the time-resolved surfaces to 2.5 ps.

exponential component peaks at 615 and 700 nm and has a broad negative feature between 500 and 600 nm.

Discussion

Electronic Structure. To understand the interplay between the nuclear and electronic coordinates in lutetium bisphthalocyanine, it is important to have a clear picture of the electronic structure of the complex. The simple changes in the absorption spectra between LuPcAc and $LuPc_2^-$ seen in Figure 1 hide complex changes in the electronic structure of the dimer. In the simplest analysis, the two monomer excited states mix to form two exciton states, $|EX+\rangle$ and $|EX-\rangle$, evenly distributed around the monomer excited state energy. However, the perpendicular degenerate transitions found in the phthalocyanine monomers would generate an optically forbidden lower exciton state, meaning this simplest view does not apply.[28]

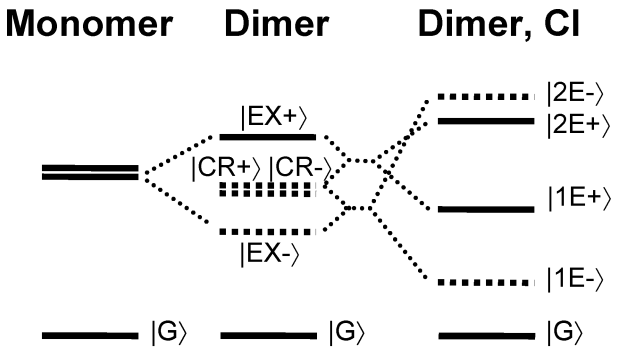

Figure 6. Schematic depiction of the electronic structure of the monomer, the dimer, and the dimer with configuration interaction (CI). States with dashed lines are dark states. See text for details. This diagram does not quantitatively depict the energies of the various levels.

A more complete analysis, including configuration interaction, indicates that the observed spectrum arises from charge transfer interactions in addition to the excitonic interactions.[20] Figure 6 schematically depicts the electronic structure we now describe. In addition to the exciton states described above, degenerate charge transfer states arise, and these interact to form symmetric, $|CR+\rangle$, and anti-symmetric, $|CR-\rangle$, charge resonance states. These charge resonance states then mix with the two exciton states. The two bands in the dimer absorption spectrum are associated with the mixing of the dipole-allowed $|EX+\rangle$ state and the dipole-forbidden $|CR+\rangle$ state. The resultant upper state, $|2E+\rangle$, is located around 16 250 cm^{-1} (615 nm) and is dominated by contributions from the allowed $|EX+\rangle$ state, while the resultant lower state, $|1E+\rangle$, is centered near 14 250 cm^{-1} (700 nm) and is composed primarily of the $|CR+\rangle$ state. Since neither the $|EX-\rangle$ state nor the $|CR-\rangle$ state has dipole strength, transitions to the two states generated by their interaction, $|1E-\rangle$ and $|2E-\rangle$, are dipole forbidden.

The degree of mixing between the charge resonance and exciton states can be extracted from electronic structure calculations and matches the values extracted from the absorption spectrum and from two-color photon echo peak shift experiments.[22]

Wave Packet Dynamics. The major oscillation we observe in our pump−probe experiments is due to a single intramolecular vibrational mode, which has a frequency of 159 cm^{-1}, corresponding to a period of 209 fs. The precise nature of this mode is unknown. Phthalocyanines are known to contain both symmetric and nonsymmetric nitrogen−metal (N−M) modes in the low frequency region.[29,30] Generally, wave packets are only observed for totally symmetric modes. For example, in work on SnPc crystals, a 190 cm^{-1} vibration is assigned to a totally symmetric doming mode.[31,32] However, recent time-resolved anisotropy experiments on naphthalocyanines indicate the presence of a wave packet from a nontotally symmetric mode, which breaks the degeneracy of the ring.[33] This nontotally symmetric mode is coupled to the transition through a frequency shift as opposed to the common displacement of equilibrium position used for symmetric modes.

As mentioned above, the most striking feature of the data is the anti-correlated modulation of the time-resolved spectra which results from the wave packet motion. Anti-correlated oscillations centered at two different spectral regions have been observed in monomeric systems.[4,5] In these cases, the anti-correlated dynamics are due to two separate wave packets, one each in the excited and ground states, whose motions are out of phase. The relative phases of the ground and excited state wave packets depend on the pump wavelength; thus, selection of a pump wavelength to the blue of the absorption maximum often shifts the relative phase, generating correlated motion of the two wave packets.

The oscillations in $LuPc_2^-$ are distinct from these systems in at least two respects. First, there are transitions between the ground state and two separate excited states rather than to two regions of a single excited state. Thus, the two oscillatory regions are not necessarily due to two separate wave packets. Second, the anti-correlated dynamics appear regardless of the pump wavelength. This second observation is supported by the data in Figure 3 but was further tested by repeating the experiment with pump wavelengths above, at, and below the maximum of each absorption band; in each case, the dynamics are anti-correlated. These persistent anti-correlated dynamics, and the fact that the frequency and dephasing of the oscillations is essentially the same throughout the spectrum, allow us to conclude that the dominant contribution to all of the observed oscillations is a single coherently excited nuclear wave packet.

Given the spectral position of the oscillations, they are most likely due to a ground state wave packet, which modulates the bleaching of the ground state absorption to both excited states. A ground state wave packet gives rise to anti-correlated dynamics when the two excited states are displaced in opposite directions along the nuclear coordinate, and we believe that this is the most likely source of the observed anti-correlated dynamics. An additional point which supports a ground state wave packet is resonance Raman data for $LuPc_2^-$ in ethanol, which shows a broad, strongly coupled mode around 160 cm^{-1}.

While we believe a ground state wave packet is the most likely scenario, we will briefly examine the possibility of a single excited state wave packet. The wave packet could exist in $|1E+\rangle$, and the modulation would be of excited state absorption at 615 nm and stimulated emission at 700 nm; alternatively, the wave packet could exist in a lower dark state, and the modulation would be of excited state absorption at both 615 and 700 nm. In the first case, the displacement of the upper excited state that would lead to the observed anti-correlated motion would be in the same direction but with greater magnitude than $|1E+\rangle$; in the second case, the two upper excited states would be displaced in opposite directions around the dark state containing the wave packet. The location of excited state absorption signals in identical spectral positions as ground state bleaches seems somewhat unlikely, but given the possible existence of a two-exciton state, it is not impossible.

For either of these excited state wave packet models, the phase of the wave packet would depend on which state is pumped, unless the nuclear coherence is maintained during at least one electronic relaxation process. Jean and Fleming showed that nuclear coherence can be maintained for electronic relaxation times less than one-quarter of a vibrational period, which is 50 fs in this case.[34] The relaxation we observe in $LuPc_2^-$ is on this time scale, so there is a possibility that this system is one of the rare ones which maintains nuclear coherence during ultrafast relaxation. Coherent nuclear motion has been observed in the product states after the isomerization of rhodopsin by Wang et al.,[8] the fragmentation of I_3^- by Banin and Ruhman,[35] and charge recombination in a tetracyanoethylene−pyrene complex by Wynne et al.[36]

For the remainder of this section, we assume that the wave packet is located in the ground state. We asserted above that, in the case of a ground state wave packet, the excited states $|1E+\rangle$ and $|2E+\rangle$ must be displaced in opposite directions in the nuclear coordinate about the ground state. However, $|1E+\rangle$ and $|2E+\rangle$ are composed of multiple underlying states and are delocalized; thus, it is not clear what a displacement of these states in the nuclear coordinate would mean. To clarify the behavior of these mixed states with respect to the nuclear coordinate, we construct a model in which the underlying electronic states, $|EX+\rangle$ and $|CR+\rangle$, are linearly coupled to the nuclear coordinate. The interaction between them, V_{EX-CR}, is also linearly coupled to the nuclear coordinate. This model will allow us to simulate the time-resolved spectra and draw conclusions about the behavior of the states and interactions and how they relate to the nuclear coordinate.

To approximately match the experimental data, the transition energies $|EX+\rangle$ and $|CR+\rangle$ are set to $E^0_{EX+} = 15\,638$ and $E^0_{CR+} = 14\,866$ cm^{-1}, and the initial interaction strength, V^0_{EX-CR}, is set to 923 cm^{-1}. These each couple to a single vibrational coordinate, x, with linear coupling strengths ΔE_{EX+}, ΔE_{CR+}, and ΔV_{EX-CR}:

$$E_{EX+} = E^0_{EX+} + \Delta E_{EX+} x \tag{1}$$

$$E_{CR+} = E^0_{CR+} + \Delta E_{CR+} x \tag{2}$$

$$V_{EX-CR} = V^0_{EX-CR} + \Delta V_{EX-CR} x \tag{3}$$

We will assume only linear couplings in this model, although the range of modulated wavelengths on the high energy side of the upper band may be evidence for nonlinear coupling. In this model, if any of the linear coupling terms are nonzero, transition strength dependence on the nuclear coordinate (non-Condon effects) can appear, as will be demonstrated below. The energies and interaction strengths from eqs 1−3 can be used to generate new mixed states, $|2E+\rangle$ and $|1E+\rangle$. The expressions used to

generate these states are as follows:

$$\tan(2\theta) = \frac{2V_{EX-CR}}{E_{EX+} - E_{CR+}} \quad (4)$$

$$|2E+\rangle = \cos(\theta)|EX+\rangle + \sin(\theta)|CR+\rangle \quad (5)$$

$$|1E+\rangle = -\sin(\theta)|EX+\rangle + \cos(\theta)|CR+\rangle \quad (6)$$

$$E_{2E+} = \sqrt{V_{EX-CR}^2 + \left(\frac{E_{EC+} - E_{CR+}}{2}\right)^2} + \frac{E_{EX+} + E_{CR+}}{2} \quad (7)$$

$$E_{1E+} = \sqrt{V_{EX-CR}^2 + \left(\frac{E_{EX+} - E_{CR+}}{2}\right)^2} + \frac{E_{EX+} + E_{CR+}}{2} \quad (8)$$

$$f_{2E+} = f_T \cos^2\theta \quad (9)$$

$$f_{1E+} = f_T \sin^2\theta \quad (10)$$

The band corresponding to each state is treated as a Gaussian in frequency space with centers E_{1E+} and E_{2E+} and transition strengths f_{1E+} and f_{2E+}. We will initially assume the total transition strength, f_T, is a constant equal to 1, with $f_T = f_{1E+} + f_{2E+}$. The width of each band is chosen to best match experiment. θ describes the degree of mixing between the $|EX+\rangle$ and $|CR+\rangle$ states to form $|1E+\rangle$ and $|2E+\rangle$ and depends on the initial state energies as well as the interaction strength. Note that any changes in the mixing will also appear as changes in the transition strengths, f_{1E+} and f_{2E+}. Non-Condon effects appear whenever there is a change in the mixing between the states, given by twice the interaction strength divided by the energy gap. On the basis of the results of our fitting, the dimensionless nuclear coordinate, x, is a function of time given by a damped cosine ranging from 1 to -1 with a period of 209 fs and a damping time of 1200 fs.

Within this model, the unknown parameters are the terms which control the coupling of the nuclear coordinate to the state energies and their interaction, namely, ΔE_{EX+}, ΔE_{CR+}, and ΔV_{EX-CR}. In effect, varying these parameters in this simple model generates new potential curves for $|1E+\rangle$ and $|2E+\rangle$ as a function of the nuclear coordinate, x. Assigning different signs to ΔE_{EX+} and ΔE_{CR+} corresponds to displacing these excited states in opposite directions with respect to the ground state equilibrium position. This leads to opposite displacements of the $|1E+\rangle$ and $|2E+\rangle$ states, since they have predominantly $|CR+\rangle$ and $|EX+\rangle$ character, respectively. The coordinate dependence of the interaction strength between $|EX+\rangle$ and $|CR+\rangle$, ΔV_{EX-CR}, also effectively contributes to displacing the $|1E+\rangle$ and $|2E+\rangle$ states in opposite directions with respect to the ground state minimum.

Figure 7 shows a series of time-resolved spectra calculated for representative parameter values. If either $|EX+\rangle$ or $|CR+\rangle$ is coupled to the vibration—as in Figure 7A, where $\Delta E_{CR+} = 100$ cm^{-1}, $\Delta E_{EX+} = 0$ cm^{-1}, and $\Delta V_{EX-CR} = 0$ cm^{-1}—both E_{1E+} and E_{2E+} move in a correlated manner because the mixing links both final energies to, in this example, changes in E_{CR+}. Weak non-Condon effects appear as stronger modulation at frequencies between the bands than those above or below the two bands. Also note that, although the linear coupling strength was set to 100 cm^{-1}, the apparent shift is significantly less because the coupling is divided between the bands.

When both E_{EX+} and E_{CR+} are linearly coupled to the nuclear coordinate with the same sign and magnitude, there is no change in mixing because the energy gap between $|EX+\rangle$ and $|CR+\rangle$ does not change. Thus, E_{1E+} and E_{2E+} move together, and the transition moments follow standard Condon behavior. When the magnitudes of the linear coupling are different, the motions of E_{1E+} and E_{2E+} are still correlated, as shown in Figure 7B, where $\Delta E_{CR+} = 100$, $\Delta E_{EX+} = 50$ cm^{-1}, and $\Delta V_{EX-CR} = 0$ cm^{-1}. In this case, there is a very slight change in mixing, associated with the change in energy gap between $|EX+\rangle$ and $|CR+\rangle$.

When the linear coupling terms have opposite signs, E_{1E+} and E_{2E+} are anti-correlated. An example of this is shown in Figure 7C, where $\Delta E_{CR+} = 100$, $\Delta E_{EX+} = -100$ cm^{-1}, and $\Delta V_{EX-CR} = 0$ cm^{-1}. The coordinate dependence of the transition strength can clearly be seen in this case: the modulation of $|1E+\rangle$ is almost negligible on the red side of the band, while the modulation is significant on the blue side. If the linear coupling terms have opposite signs but different magnitudes, the results are different again. Figure 7D shows this for $\Delta E_{CR+} = 100$, $\Delta E_{EX+} = -50$ cm^{-1}, and $\Delta V_{EX-CR} = 0$ cm^{-1}. With these parameters, interactions between $|EX+\rangle$ and $|CR+\rangle$ cause the cancellation of the change in E_{2E+}, making it nearly constant in time. These parameters do generate a coordinate dependence in the transition strength, f_{2E+}, associated with the change in the degree of mixing between $|EX+\rangle$ and $|CR+\rangle$. When only the interaction strength is coupled to the nuclear mode, E_{1E+} and E_{2E+} are anti-correlated. Figure 7E shows this for $\Delta E_{EX+} = 0$, $\Delta E_{CR+} = 0$, and $\Delta V_{EX-CR} = 100$ cm^{-1}. This yields a nuclear dependence of the transition strength which is barely visible in the simulated spectrum.

In this simple model, the best fit parameters are $\Delta E_{EX+} = -60$, $\Delta E_{CR+} = 60$, and $\Delta V_{EX-CR} = 30$ cm^{-1}, as shown in Figure 7F. With these parameters, the motion of E_{1E+} and E_{2E+} is anti-correlated, as seen in the experiment, and there is weaker modulation on the blue edge of the $|2E+\rangle$ band. The difference in signs for ΔE_{EX+} and ΔE_{CR+} indicates a possible assignment of the nuclear coordinate to a modulation of the effective distance between the phthalocyanine rings. As the rings approach each other, the energy of the upper exciton state would increase due to increased exciton coupling; meanwhile, the energy of the charge resonance state would decrease due to smaller charge separation for the underlying charge transfer states.

To more quantitatively show the effects of the different linear couplings on the transition strengths and energies, we have included Table 1. This table lists the transition energies and transition strengths at the turning points ($x = 1, -1$) of the nuclear coordinate compared to their values at the equilibrium nuclear position ($x = 0$) for a series of values for the linear coupling parameters. For $x = 0$, E_{E1+}, E_{E2+}, f_{E1+}, and f_{E2+} are 14 252 cm^{-1}, 16 252 cm^{-1}, 0.3071, and 0.6929, respectively. Because the total transition strength in this model is constant, only the change for f_{1E+} is shown. We note that, while the energies and interaction strength were each linearly coupled to the nuclear mode, the electronic interactions between the states generate a nonlinear response to the nuclear motion. This can be seen in Table 1 by comparing the difference for the positive and negative turning points for x. For example, in the case which matches Figure 7C (the fifth line in Table 1), the transition frequencies from the ground state to the $|1E+\rangle$ state at the turning points of the wave packet relative to the center point for the wave packet are -43 and 34 cm^{-1}; if the response was linear, the magnitudes of the change would be identical.

If the model developed in eqs 4−10 is sufficient to describe the system, the total integrated transient absorption signal should show no dependence on the nuclear coordinate (f_T will be constant), although the transition strength will shift between the two bands. Thus, the integration of the total signal should not

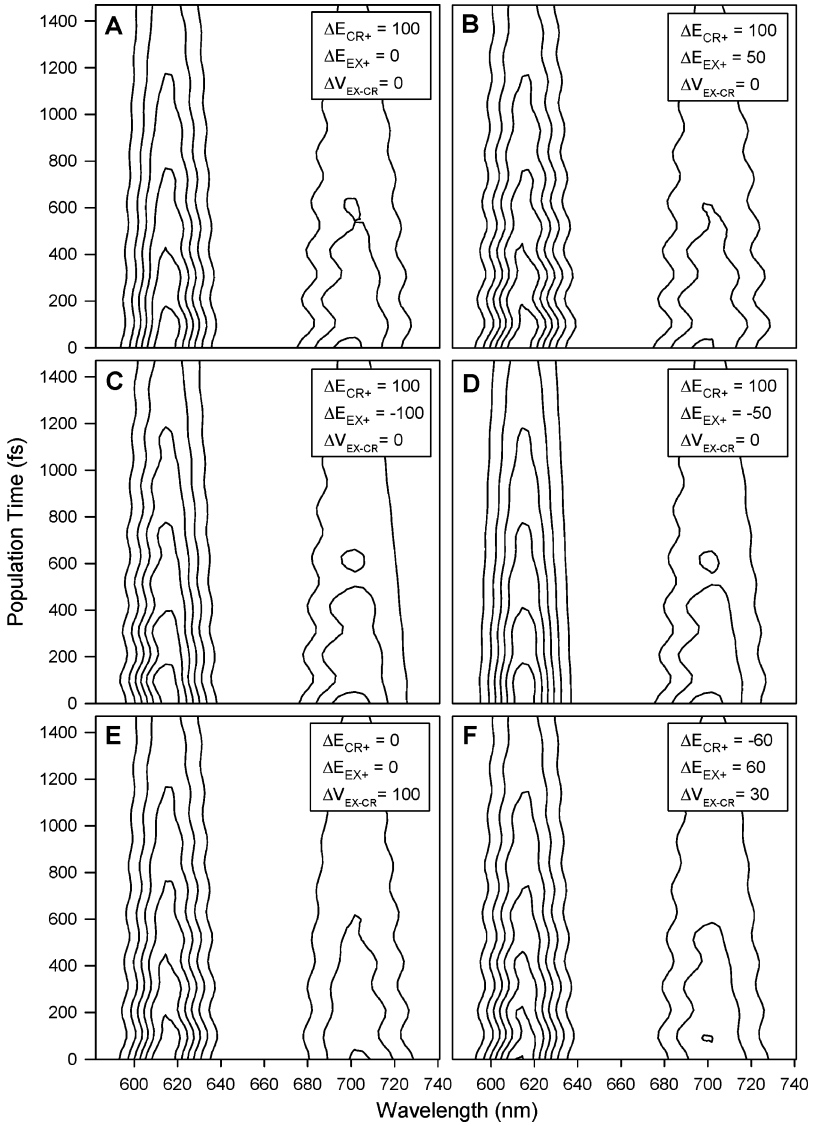

Figure 7. Simulations based on eqs 1−10. Parameters common to all panels are given in the text; those that vary (the linear coupling strengths) are given on each panel.

TABLE 1: Effect of Linear Coupling Parameters on Excited State Energies and Transition Strengths

	ΔE_{CR+}	ΔE_{EX+}	ΔV	$\Delta E_{1E}(-1)$	$\Delta E_{1E}(1)$	$\Delta E_{2E}(-1)$	$\Delta E_{2E}(1)$	$\Delta f_{1E}(-1)$	$\Delta f_{1E}(1)$
a[a]	100[b]	0	0	−71	68	−29	32	−0.0207	0.0219
	0	100	0	−32	29	−68	71	0.0219	−0.0207
	100	100	0	−100	100	−100	100	0	0
b	100	50	0	−85	84	−65	66	−0.0105	0.0108
c	100	−100	0	−43	34	43	−34	−0.0401	0.0449
d	100	−50	0	−57	51	7	−1	−0.0305	0.0332
e	0	0	100	91	−93	−91	93	−0.0194	0.0164
	0	−50	50	60	−63	−10	13	−0.0201	0.0190
	50	−50	50	24	−29	−24	29	−0.0305	0.0297
f	−60	60	30	49	−52	−49	52	0.0214	−0.0190

[a] The left column denotes the panel of Figure 7 corresponding to these parameters. [b] Energies are given in wavenumbers (cm^{-1}).

contain oscillations. The result of this integration for our experimental data is shown in Figure 8. The integrated area of the entire transient absorption spectra shows noticeable oscillation with a period of approximately 210 fs, which indicates additional non-Condon dynamics for which our simple model does not account.

One source of coordinate dependence in the overall transition strength is the underlying structure of the $|EX+\rangle$ state. If the 210 fs mode changes the interaction between the locally excited states, the transition strength of the $|EX+\rangle$ state could be modified. It is known from one-color photon echo peak shift experiments (1C3PEPS) that the monomer contains a vibration with a frequency similar to that seen in the dimer, implying that the energies of the states which make up the $|EX+\rangle$ state are coupled to this mode.[37]

Setting aside the oscillations in transition strength for a moment, Figure 8 also shows that the total transition strength is divided almost evenly between the two bands. The value of f_{2E+} would be expected to be approximately twice that of f_{1E+}, since it represents over half of the total transition strength. The

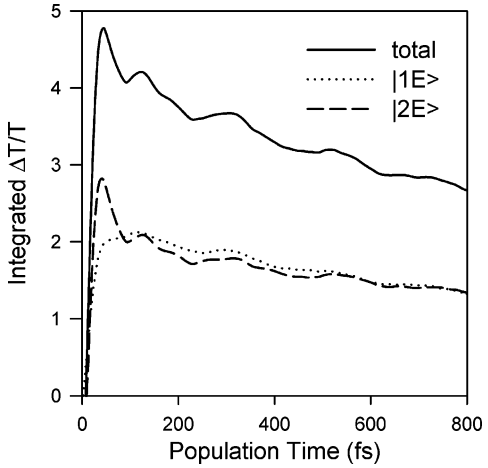

Figure 8. Integration with respect to the frequency of the total spectrum (solid line) and of the $|2E+\rangle$ (dotted line) and $|1E+\rangle$ (dashed line) bands as a function of population time.

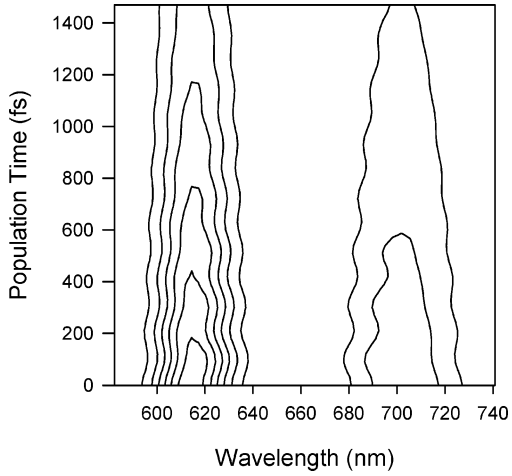

Figure 9. Simulations based on eqs 1−11 using the parameter set that best matches the experimental data: -25 cm^{-1}, 25 cm^{-1}, 26 cm^{-1}, and -0.03 for ΔE_{CR+}, ΔE_{EX+}, ΔV_{EX-CR}, and Δf_T, respectively, with initial transition energies of 15 638 and 14 866 cm^{-1} for $|EX+\rangle$ and $|CR+\rangle$ and an initial interaction strength, V_{EX-CR}, of 923 cm^{-1}.

departure from this 2 to 1 ratio in Figure 8 is explained by the excited state absorption in the region between 500 and 600 nm, which cancels some of the signal associated with the bleach on the $|2E+\rangle$ state.

Returning to the oscillations in transition strength, the sizes of the oscillations for the two individual bands are also the same, and the modulation is correlated modulation. If the coordinate dependence of the transition strengths could be assigned merely to a change in the overall transition strength, f_T, the amplitude of oscillations of f_{2E+} would be expected to be approximately twice that of f_{1E+}, but in this case, the presence of excited state absorption, which is expected to be relatively constant, does not explain the discrepancy. Rather, it is likely that the mixing of $|EX+\rangle$ and $|CR+\rangle$ varies in a way which allows the change in f_{2E+} associated with mixing to partially cancel the change in f_{2E+} associated with the total transition strength, causing a lower than expected modulation amplitude.

To incorporate the oscillations in total transition strength into our previous model, we add the following equation:

$$f_T = 1 + x\Delta f_T \tag{11}$$

On the basis of the data in Figure 8, the magnitude of the linear coupling strength of the total transition strength to the nuclear coordinate, Δf_T, is approximately 0.03. When including this new equation, it is important to understand the effect of various parameters on the transition strength of each band, f_{2E+} and f_{1E+}. As shown in eqs 9 and 10, these transition strengths depend on the nuclear coordinate, x, not only through their dependence on f_T but also through their dependence on θ. In turn, θ is a complicated function of the nuclear coordinate, because of its dependence on all three linear coupling parameters, ΔE_{CR+}, ΔE_{EX+}, and ΔV_{EX-CR}.

Because Δf_T is fixed by the data, these remaining parameters must be varied in order to not only match the oscillations in the data (as was done to generate Figure 7) but to also match the oscillations in the transition strengths of the individual bands. Adding only ΔV_{EX-CR}, or both ΔE_{CR+} and ΔE_{EX+}, without Δf_T does not produce a good fit of the data, because the magnitude necessary to produce the correct form of the oscillations results in oscillations in transition strength that are much too large. Correct selection of the signs for the linear coupling parameters allows the change in θ, and thus the size of the oscillations in the transition strength, to be minimized, while maintaining the proper amplitudes for the oscillations in the signal.

The parameter set that best fits the data, resulting in Figure 9, is as follows: $\Delta E_{CR+} = -25$ cm^{-1}, $\Delta E_{EX+} = 25$ cm^{-1}, $\Delta V_{EX-CR} = 26$ cm^{-1}, and $\Delta f_T = -0.03$. In this model, the initial transition energies of $|EX+\rangle$ and $|CR+\rangle$ are set at 15 638 and 14 866 cm^{-1}, and the initial interaction strength, V^0_{EX-CR}, is set at 923 cm^{-1}. Since the degree of mixing between the two states depends on the ratio of the interaction strength and the energy gap, these values for the linear coupling strengths limit the change in mixing induced as the nuclear coordinate moves because the interaction strength decreases as the energy gap decreases. The calculated signal in Figure 9 matches most of the experimental data in Figure 2 very well: it shows anticorrelated wave packet dynamics and matches the slightly asymmetric appearance for the modulation of the $|1E+\rangle$ band as seen in Figure 2. Figure 9 does not match the very asymmetric appearance of the $|2E+\rangle$ wave packet which, as noted above, likely arises from nonlinear coupling. Nonlinear coupling of the nuclear coordinate to the underlying energies and the interstate interaction would not be surprising, since the two interacting states, $|EX+\rangle$ and $|CR+\rangle$, are derived from mixed states. For example, nonlinear coupling could arise if the nuclear coordinate involved the intermolecular distance, which could influence the overlap of orbitals with exponential tails, or the x^3 dipole−dipole coupling between monomers.

The model we developed here is similar in many respects to one developed to describe wave packets observed in SnPc crystals.[31] In that system, regions of a single broad absorption band are assigned to charge transfer (CT) and exciton (EX) states. The CT region shows a modulation in transient absorption intensity at a frequency of 190 cm^{-1} with a nearly uniform phase,[32] which the authors assigned to changes in the mixing between the CT and EX states which affect mainly the transition strength of the CT band. The absence of modulation in the EX region of the band is probably due to the EX transition's strength being much larger than that of the CT state; thus, the same absolute level of modulation is dominated by other dynamics. In our experiments, modulation is observed in the transition energies and strengths of both bands, clearly indicating complex mixing phenomenon between the $|EX+\rangle$ and $|CR+\rangle$ states.

One major shortcoming of our model is that it does not clearly explain the lack of sensitivity of the overall wave packet phase to the pump wavelength. As mentioned above, the overall phase of all oscillations is identical, regardless of pump wavelength,

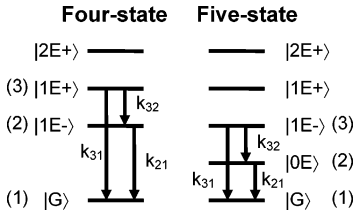

Figure 10. Kinetic model for excited state relaxation in $LuPc_2^-$. When using either a four- or five-state model, the relevant dynamics involve only three states after fast relaxation from higher states (see text for details).

to within our time resolution. Assuming, as we have done, that the excited states are displaced in opposite directions from the ground state, a π phase shift is expected for pumping $|1E+\rangle$ versus $|2E+\rangle$ because the momentum imparted to the wave packet would be in opposite directions.[4,5,7,38,39]

The lack of phase shift for different pump wavelengths could be due in part to the non-Condon effects described above. In the presence of non-Condon effects, the distribution of a wave packet (in either the ground or excited state) along the nuclear coordinate is different than what would be expected on the basis of the initial ground state distribution, a coordinate-independent transition moment, and the spectrum of the excitation pulse. It is unclear whether the non-Condon effects included in the model above are strong enough to influence the wave packet formation. It is possible that the complicated electronic structure of the excited state may influence the formation of the ground state wave packet in a manner not trivially derived from calculations on two-level systems. For example, the interaction between the nuclear and electronic states will lead to a breakdown of the Born−Oppenheimer approximation.

Excited State Relaxation Dynamics. We now move to an analysis of the excited state relaxation dynamics of $LuPc_2^-$. Our analysis will have two goals. First, we wish to find evidence which will allow us to confirm the ground state as the location of the wave packet. Second, because the time resolution of our experiments is several orders of magnitude higher than that used previously to study lanthanide bridged dimers, our analysis will yield new information about the excited state dynamics of this system.

The presence of two pump-independent time scales, 1.5 and 11 ps, indicates more complex relaxation dynamics than expected in a three-state model consisting of one ground state and two excited states ($|G\rangle$, $|1E+\rangle$, and $|2E+\rangle$). At least one additional state below $|1E+\rangle$ is required to explain the observed dynamics. Electronic structure calculations predict that a state, $|1E-\rangle$, produced by mixing the $|EX-\rangle$ and $|CR-\rangle$ states, exists at a lower energy than $|1E+\rangle$.[20] The presence of such a state around 9000 cm^{-1} is also suggested by very weak absorbance in the linear spectrum.[40] In this basic four-state model, the system undergoes rapid relaxation from $|2E+\rangle$ to $|1E+\rangle$ and then to the ground state, with at least some of the population passing through $|1E-\rangle$. A level diagram for this case is displayed on the left-hand side of Figure 10.

This four-state model fits the experiment, but it does require that excitation remain in the dipole-allowed $|1E+\rangle$ state for a significant amount of time, on the order of 1.5 ps. This lifetime corresponds to a detectable quantum yield, on the order of 10^{-4}, but steady state fluorescence for this system has not been reported in the wavelength range of $|1E+\rangle$ (around 700 nm). Our fluorescence measurements indicate that the quantum yield is not above 10^{-4} but did not yield an upper bound for the quantum yield smaller than that value.

If this molecule is not fluorescent in this spectral region, a fifth state, which we will denote as $|0E\rangle$, is needed to explain the dynamics. A level diagram for this case is displayed on the right-hand side of Figure 10. Fast (~100 fs) decay from $|1E+\rangle$ to $|1E-\rangle$ on the order of 100 fs would reduce the $|1E+\rangle$ fluorescence quantum yield to 10^{-5} and could easily be masked by the vibrational dynamics. The population then decays from $|1E-\rangle$, partially through $|0E\rangle$, to the ground state, $|G\rangle$.

Since relaxation faster than the time resolution of our experiment moves all population to three lower states for both the four- and five-state models, only three states are used in our kinetic equations. Again, refer to Figure 10 for level diagrams corresponding to each model. In both the four- and five-state models, state 1 is the ground state. In the four-state model, state 2 corresponds to the $|1E-\rangle$ state and state 3 corresponds to the $|1E+\rangle$ state. In the five-state model, state 2 corresponds to the $|0E\rangle$ state and state 3 corresponds to the $|1E-\rangle$ state. The observed signal is the sum of the ground state bleach (GSB) associated with the loss of population in the ground state, 1, the excited state absorption (ESA) from both intermediate states, 2 and 3, and the possible stimulated emission (SE) of the upper intermediate state, 3.

To estimate the yields along the various decay pathways, we first determine the relative contributions of ground state bleach and state 3 excited state absorption to the spectrally resolved signal. We model the ground state bleach by scaling the ground state linear absorption spectrum. The excited state absorption is then determined by the difference between the observed spectrally resolved signal and the ground state bleach. Figure 11A and B shows the ground state bleach and excited state absorption spectra generated for two possible values of the total initially excited state 3 population. In either the four- or five-state model, the negative signal generated in the region of the $|2E+\rangle$ absorption (~615 nm) must be given by the ground state bleach signal. In Figure 11A, this minimum value of initially excited population is used, but whereas excited state absorption bands are generally broad and featureless, the state 3 spectrum in this panel has considerable structure. Figure 11B shows the same spectra for a value of state 3 initial population which is sufficiently large to produce a nearly featureless excited state absorption spectrum for state 3.

The amount of population transferred to state 2 can also be estimated; Figure 11C and D shows this excited state absorption spectrum for different values of population transfer to state 2. Figure 11C shows the state 2 excited state absorption for a small amount of population transfer. This spectrum shows a very structured region around 610 nm, which would be unusual for an excited state absorption spectrum. A population transfer large enough to generate a smoother ESA is shown in Figure 11D. The resulting spectrum is very similar to a red-shifted ground state absorption spectrum, and it could be associated with either a hot ground state species or an exciton state where absorption to the bi-exciton state is red-shifted from the single exciton absorption.

The values which give appropriate excited state absorption spectra generate a yield of 0.6 for direct relaxation from state 3 to the ground state and 0.4 for relaxation through state 2. This represents a lower limit on the relaxation through state 2, since additional remaining bleach would shift the ESA closer toward the bleach without changing its structure. These estimates for the initial population excited to state 3 and the transfer yield to state 2, along with the 1.5 ps lifetime for state 3, yield values for the rate constant displayed in Figure 10 of 0.26 ps^{-1} for k_{32} and 0.4 ps^{-1} for k_{31}.

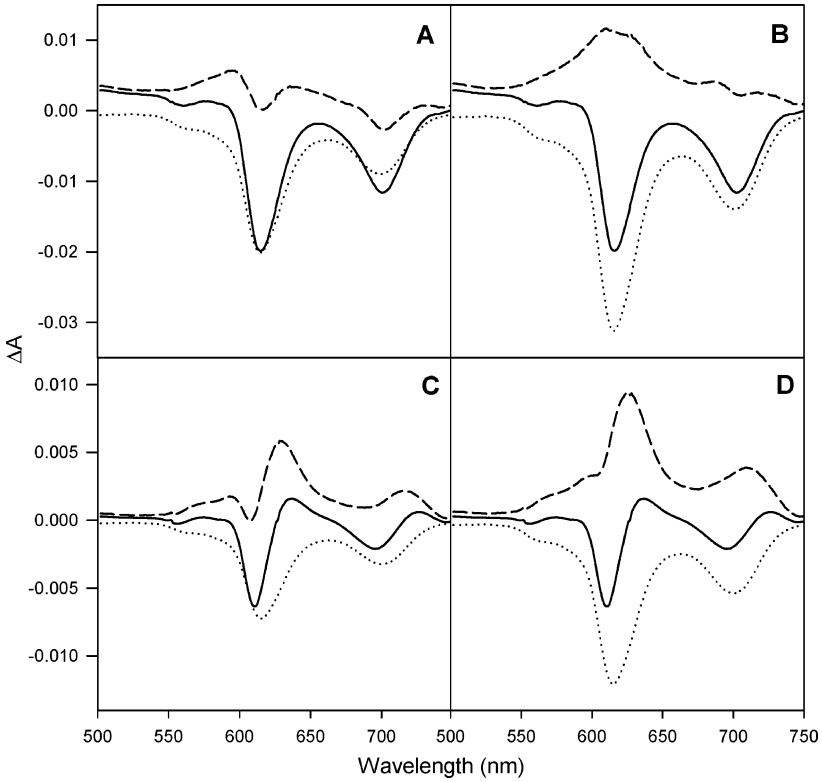

Figure 11. Time-resolved spectrum (solid line) and its component spectra: the ground state bleach (dotted line) and the state 3 (panels A and B) or state 2 (panels C and D) excited state absorption. Panels A and B show the time-resolved spectrum at time zero and component spectra for a minimum and a larger value of initially excited state 3 population, respectively. Panels C and D show the time-resolved spectra after the initial decay (taken to be the static component shown in Figure 5) and component spectra for a minimum and a larger value of population decay through state 2, respectively.

While phthalocyanine molecules have been studied extensively, excited state relaxation dynamics in lanthanide bridged dimers have received little attention. Studies using pulses on the order of 20 ps performed on $LuPc_2$ in three oxidation states yielded a single exponential fit of less than 36 ps for $LuPc_2^-$, with a spectral response similar to the 11 ps component in our experiment.[41] Silicon μ-oxo bridged phthalocyanine complexes, including dimers, trimers, and multimers, have been studied by several authors.[42−44] The time scales observed in two of these studies are found to be significantly slower than those observed here, with a dominant time scale of 100−200 ps and considerable generation of triplet states which decayed on a microsecond time scale.[43,44] In the third study, the phthalocyanine rings were chemically modified to improve solubility, which significantly affected the absorption spectrum of the dimer, making it broad with considerable structure, possibly resulting from inhomogeneous broadening from a distribution of dimer structures.[42] Associated with this spectral change is the appearance of a fast relaxation time scale of 7 ps, which was attributed by the authors to relaxation from an electronic state around 9000 cm^{-1} (the $|1E-\rangle$ state in our model) to a triplet state mediated by the charge resonance component of the state. This triplet state then decays to the ground state on a 150 ps time scale.

All of these studies found an initial relaxation on a time scale faster than the instrument response to a low lying state below the $|1E+\rangle$ state. This is then followed by relaxation with a time scale around 100 ps to the ground state. This supports the five-state model for the relaxation dynamics (see Figure 10), where $|0E\rangle$ represents a hot ground state or a ground state isomer.

Returning to the question of the location of the wave packet, the five-state model supports the placement of the wave packet in the ground state. In the five-state model, if the wave packet were in the excited state, the nuclear coherence would have to survive two relaxation steps when the pump beam is resonant with the $|2E+\rangle$ state; in addition, there would have to be excited state absorption to two separate states at frequencies nearly identical to those of the ground state bleach. While none of these occurrences are impossible, the ground state wave packet seems more plausible.

Conclusion

The ultrafast dynamics of a phthalocyanine dimer have been studied with femtosecond transient absorption spectroscopy. A coherently excited nuclear wave packet, with a frequency of 159 cm^{-1}, generates anti-correlated motion in the transient spectrum. The wave packet is most likely located in the ground state, and the anti-correlated motion indicates that the interactions between the charge resonance and exciton states are modulated by the nuclear mode. The presence of such mixing has previously been verified using two-color photon echo peak shift experiments.[22,23] There is also a possibility that the wave packet is formed in an excited state after maintaining nuclear coherence during one or more electronic relaxation steps.

To properly describe the oscillations in the data, a model was developed which includes changes in the mixing between the two states caused by linear coupling of their energies and their interaction strength to the vibrational mode. It was found that a balance between the anti-correlated shifts in energies and change in interaction strength can reproduce most of the critical features of the data. Additional nonlinear coupling can explain the remaining features. We are not able to account for the pump-wavelength independence of the overall phase of the wave packet in our simple model, but the complicated structure of the excited electronic states would be expected to influence wave packet formation and generate a breakdown of the Born−Oppenheimer approximation.

The first relaxation step could not be resolved with our 50 fs instrument response. The observed later relaxation dynamics of the excited state occur on two time scales: 1.5 and 11 ps. A three-level model is used to describe the kinetics with both sequential and direct relaxation mechanisms after unresolved relaxation. The identical decay kinetics seen for pumping the two states and the presence of excited state absorption around the 615 nm band will be useful for further modeling of 2C3PEPS experimental results. This experiment could then reveal how the coupling between the two different types of states, charge resonance and exciton, is influenced by their different interactions with the bath.

Our findings may be relevant to the study of the special pair in bacterial photosynthetic reaction centers,[24−26] for which bisphthalocyanine could be considered a model, and where the interaction of charge transfer states and exciton states has recently been proposed to account for the unusual temperature dependence of the absorption bands.[3] As seen in $LuPc_2^-$, the change in the mixing between electronic states induced by the nuclear dynamics may influence charge separation or other excited state dynamics in the photosynthetic reaction center.[45,46]

Acknowledgment. We thank Philipp Kukura and Richard Mathies for providing a low frequency resonance Raman spectrum of the $LuPc_2^-$ in ethanol. Funding for this work was provided by NSF.

References and Notes

(1) Hoff, A. J.; Deisenhofer, J. *Phys. Rep.* **2004**, *287*, 2.
(2) van Amerongen, H.; Valkunas, L.; van Grondelle, R. *Photosynthetic Excitons*; World Scientific Publishing: Singapore, 2000.
(3) Renger, T. *Phys. Rev. Lett.* **2004**, *93*, 188101.
(4) Kumar, A. T. N.; Rosca, F.; Widom, A.; Champion, P. M. *J. Chem. Phys.* **2001**, *114*, 701.
(5) Kumar, A. T. N.; Rosca, F.; Widom, A.; Champion, P. M. *J. Chem. Phys.* **2001**, *114*, 6795.
(6) Yang, T. S.; Chang, M. S.; Chang, R.; Hayashi, M.; Lin, S. H.; Vohringer, P.; Dietz, W.; Scherer, N. F. *J. Chem. Phys.* **1999**, *110*, 12070.
(7) Jonas, D. M.; Bradforth, S. E.; Passino, S. A.; Fleming, G. R. *J. Phys. Chem.* **1995**, *99*, 2594.
(8) Wang, Q.; Schoenlein, R. W.; Peteanu, L. A.; Mathies, R. A.; Shank, C. V. *Science* **1994**, *266*, 422.
(9) Dhar, L.; Rogers, J. A.; Nelson, K. A. *Chem. Rev.* **1994**, *94*, 157.
(10) Pollard, W. T.; Mathies, R. A. *Annu. Rev. Phys. Chem.* **1992**, *43*, 497.
(11) Dexheimer, S. L.; Wang, Q.; Peteanu, L. A.; Pollard, W. T.; Mathies, R. A.; Shank, C. V. *Chem. Phys. Lett.* **1992**, *188*, 61.
(12) Scherer, N. F.; Carlson, R. J.; Matro, A.; Du, M.; Ruggiero, A. J.; Romero-Rochin, V.; Cina, J. A.; Fleming, G. R.; Rice, S. A. *J. Chem. Phys.* **1991**, *95*, 1487.
(13) Fragnito, H. L.; Bigot, J. Y.; Becker, P. C.; Shank, C. V. *Chem. Phys. Lett.* **1989**, *160*, 101.
(14) Zewail, A. H. *Science* **1988**, *242*, 1645.
(15) Ruhman, S.; Joly, A. G.; Nelson, K. A. *J. Chem. Phys.* **1987**, *86*, 6563.
(16) Rosker, M. J.; Wise, F. W.; Tang, C. L. *Phys. Rev. Lett.* **1986**, *57*, 321.
(17) Yan, Y. J.; Mukamel, S. *Phys. Rev. A* **1990**, *41*, 6485.
(18) Engel, M. K. Single-Crystal Structures of Phthalocyanine Complexes and Related Macrocycles. In *The Porphyrin Handbook*; Kadish, K. M., Smith, K. M., Guilard, R., Eds.; Elsevier Science: San Diego, CA, 2003; Vol. 20, p 1.
(19) Daniels, R. B.; Peterson, J.; Porter, W. C.; Wilson, Q. D. *J. Coord. Chem.* **1993**, *30*, 357.
(20) Ishikawa, N.; Ohno, O.; Kaizu, Y.; Kobayashi, H. *J. Phys. Chem.* **1992**, *96*, 8832.
(21) Ishikawa, N. *J. Porphyrins Phthalocyanines* **2001**, *5*, 87.
(22) Prall, B. S.; Parkinson, D. Y.; Fleming, G. R.; Yang, M.; Ishikawa, N. *J. Chem. Phys.* **2004**, *120*, 2537.
(23) Cho, M.; Fleming, G. R. *J. Chem. Phys.* **2005**, *123*, 114506.
(24) Allen, J. P.; Feher, G.; Yeates, T. O.; Komiya, H.; Rees, D. C. *Proc. Natl. Acad. Sci. U.S.A.* **1987**, *84*, 6162.
(25) Allen, J. P.; Feher, G.; Yeates, T. O.; Rees, D. C.; Deisenhofer, J.; Michel, H.; Huber, R. *Proc. Natl. Acad. Sci. U.S.A.* **1986**, *83*, 8589.
(26) Chirino, A. J.; Lous, E. J.; Huber, M.; Allen, J. P.; Schenck, C. C.; Paddock, M. L.; Feher, G.; Rees, D. C. *Biochemistry* **1994**, *33*, 4584.
(27) Ferro, A. A.; Jonas, D. M. *J. Chem. Phys.* **2001**, *115*, 6281.
(28) Ohno, O.; Ishikawa, N.; Matsuzawa, H.; Kaizu, Y.; Kobayashi, H. *J. Phys. Chem.* **1989**, *93*, 1713.
(29) Haghighi, M. S.; Homborg, H. *Z. Anorg. Allg. Chem.* **1994**, *620*, 1278.
(30) Haghighi, M. S.; Teske, C. L.; Homborg, H. *Z. Anorg. Allg. Chem.* **1992**, *608*, 73.
(31) Kobayashi, T.; Hirasawa, M. *J. Phys. Chem. B* **2005**, *109*, 74.
(32) Hirasawa, M.; Sakazaki, Y.; Hane, H.; Kobayashi, T. *Chem. Phys. Lett.* **2004**, *392*, 390.
(33) Farrow, D. A.; Qian, W.; Smith, E. R.; Jonas, D. M. *Abs. Pap. Am. Chem. Soc.* **2004**, *227*, U250.
(34) Jean, J. M.; Fleming, G. R. *J. Chem. Phys.* **1995**, *103*, 2092.
(35) Banin, U.; Ruhman, S. *J. Chem. Phys.* **1993**, *98*, 4391.
(36) Wynne, K.; Reid, G. D.; Hochstrasser, R. M. *J. Chem. Phys.* **1996**, *105*, 2287.
(37) Prall, B. S. Ph.D. Thesis, University of California, Berkeley, 2005.
(38) Smith, T. J.; Ungar, L. W.; Cina, J. A. *J. Lumin.* **1994**, *58*, 66.
(39) Shen, Y. C.; Cina, J. A. *J. Chem. Phys.* **1999**, *110*, 9793.
(40) Weiss, R.; Fischer, J. Lanthanide Phthalocyanine Complexes. In *The Porphyrin Handbook*; Kadish, K. M., Smith, K. M., Guilard, R., Eds.; Elsevier Science: San Diego, CA, 2003; Vol. 16, p 171.
(41) Germain, A.; Ebbesen, T. W. *Chem. Phys. Lett.* **1992**, *199*, 585.
(42) Oddos-Marcel, L.; Madeore, F.; Bock, A.; Neher, D.; Ferencz, A.; Rengel, H.; Wagner, G.; Kryschi, C.; Trommsdorff, H. P. *J. Phys. Chem.* **1996**, *100*, 11850.
(43) Pelliccioli, A. P.; Henbest, K.; Kwag, G.; Carvagno, T. R.; Kenney, M. E.; Rodgers, M. A. J. *J. Phys. Chem. A* **2001**, *105*, 1757.
(44) Fujitsuka, M.; Ito, O.; Konami, H. *B. Chem. Soc. Jpn.* **2001**, *74*, 1823.
(45) Streltsov, A. M.; Vulto, S. I. E.; Shkuropatov, A. Y.; Hoff, A. J.; Aartsma, T. J.; Shuvalov, V. A. *J. Phys. Chem. B* **1998**, *102*, 7293.
(46) Vos, M. H.; Jones, M. R.; Martin, J. L. *Chem. Phys.* **1998**, *233*, 179.